Plasmonics (2020) 15:1243–1250
https://doi.org/10.1007/s11468-020-01133-7

Theory of Optical Coupling Effects Among Surfactant Au Nanoparticles Films

David Muñetón Arboleda[1] · Marcelo Lester[2,3] · María C. Dalfovo[1] · Diana C. Skigin[4,5] · Marina E. Inchaussandague[4,5] · Francisco J. Ibañez[1]

Received: 25 October 2019 / Accepted: 27 January 2020 / Published online: 3 March 2020

Abstract

In previous reports, Dalfovo et al. showed experimentally that thin films of Au nanoparticles (NP) with organic coating change their optical properties when exposed to several analytes in the vapor phase (Anal Chem 84:4886–4892 2012; J Phys Chem C 119:5098–5106 2015). This optical behavior was associated with changes in the mean distance between nanoparticles, which resulted in a displacement of their plasmon bands towards blue or red in the presence of toluene (Tol) or ethanol (EtOH) vapors, respectively. In the report by Dalfovo et al. (J Phys Chem C 119:5098–5106 2015), in-situ grazing-incidence small-angle X-ray spectroscopy (GISAXS) was performed to determine changes in the inter-NP distance within the film. In the present work, we perform theoretical calculations to interpret the results obtained by Dalfovo et al. (Anal Chem 84:4886–4892 2012; J Phys Chem C 119:5098–5106 2015). For this purpose, we employ two different theoretical approaches, a quasi-static method (QS) and the Korringa-Kohn-Rostoker method (KKR), in order to describe the plasmon resonance shift as a function of the inter-NP distance changes during exposure to Tol and EtOH vapors. Both theoretical approaches describe qualitatively the behavior observed in previous experimental results that correlate the plasmon resonant wavelength with the inter-NP distance obtained by GISAXS. Our theoretical results show that the plasmon resonant wavelength strongly depends on the ratio between the inter-particle distance and the diameter of the nanoparticles and consequently, these films could be used for optical tuning.

Keywords Plasmon resonances · Optical tuning · Optical sensing

Introduction

Small inter-nanoparticle distance changes may lead to significant changes in the optical properties of plasmonic nanoparticles [1]. Control over the distance between NPs impact directly on applications such as LSPR sensing [2, 3] SERS [4], optical filters [5], optoelectronics [6], and energy transfer between a dye and nanoparticles for solar cells [7], just to mention a few. Most of the colorimetric applications are based on plasmonic NPs that tend to aggregate upon the presence of the analyte of interest, causing dramatic shifts in wavelength. Fundamental studies regarding coupling effects have been addressed experimentally by several groups which include Rechberger et al. [8], Haynes et al. [9], El-Sayed and co-workers [10], and more recently, Jenkins et al. [11]. Their approach is usually based on fixing NPs (at certain distances) to a desired substrate, via lithographic process, for ultimately studying plasmon shifts caused by changes in the NPs distance and in the polarization of light, performed under the same environmental conditions (i.e., dielectric medium). Other groups have protected Au NPs with organic and biological ligands in order to have a better control on the distance between metallic centers, by controlling the length of the alkyl chains [12, 13], placing

✉ Marcelo Lester
mlester@exa.unicen.edu.ar

1 Instituto de Investigaciones Fisicoquímicas, Teóricas y Aplicadas (INIFTA), Universidad Nacional de La Plata - CONICET, Sucursal 4 Casilla de Correo 16 (1900) La Plata, Argentina

2 Instituto de Física Arroyo Seco, IFAS (UNCPBA), Tandil, Argentina

3 CIFICEN (UNCPBA-CICPBA-CONICET), Grupo Óptica de Sólidos - Elfo, Pinto 399, 7000 Tandil, Argentina

4 Facultad de Ciencias Exactas y Naturales, Departamento de Física, Grupo de Electromagnetismo Aplicado, Buenos Aires, Argentina

5 CONICET - Instituto de Física de Buenos Aires (IFIBA), Universidad de Buenos Aires, Buenos Aires, Argentina

bio-molecules between dimers [14], or just by separating them with a self-assembled monolayer [15].

However, the study of coupling effects during plasmon sensing with films comprising organic-coated NPs is more challenging to monitor because NPs are arranged in a 3D configuration meanwhile the film is subjected to alterations of the refractive index every time the analyte partitions into it. For instance, in the presence of toluene, used as analyte, there is a competition between coupling effects and refractive index [2]. This is because non-polar analytes lead to swelling of the film (overall separation among NPs and therefore a blueshift of the plasmon wavelength) [3]. At the same time, toluene has a high refractive index which causes a redshift of the plasmon band.

Another challenging aspect in the field of plasmonics has been to develop accurate theoretical methods to simulate the electromagnetic response and understand light-matter interactions in more complex systems such as 2D or 3D NP films. Since Mie's solution considers an isolated NP, theoretical models dealing with more realistic systems (i.e., NPs in close proximity and arranged in complex geometrical configurations) are crucial to understand the optical response of these films [16–18]. A lot of effort has been invested into theoretical and numerical developments to describe the optical response of strongly interacting metallic NPs, mainly dimers [19, 20]. However, given the complexity of these models, the physical processes involved in the interaction are, in some cases, hidden in the numerical results.

In order to explore into the optical properties of surfactant-coated Au NP films, we employed two different approaches. On the one hand, we applied a theoretical model based on the quasi-static approximation, which permits to find an analytical expression for the dependency of the resonant frequency on the geometrical parameters of 1D and 2D arrangements of metallic NPs. On the other hand, to allow for a full 3D calculation of the electromagnetic response, we complete the theoretical treatment by using the Korringa-Kohn-Rostoker (KKR) wave calculation method which permits the study of the electromagnetic response of films formed by periodic arrays of nano-spheres embedded in a homogeneous medium [21–23]. This method has shown to be numerically efficient in the case of colloidal crystals as well as for metal-dielectric systems. It has even shown an excellent agreement with experimental results obtained at high-order band frequencies [24, 27]. We also include results obtained by the Maxwell Garnett (MG) approximation, in which the array of NPs is replaced by an effective medium slab [23, 25, 26].

With these tools at hand, we are able to perform a theoretical-numerical analysis of the experimental results described in Refs. [2, 3]. This work is organized as follows. In Section "Theoretical Methods", we present the different approaches involved in this study. In section "Quasi-static Model", we apply the quasi-static approximation to derive the equations that describe the optical response of interacting NPs forming 1D or 2D periodic arrangements, and in section "KKR Method", we summarize the basic concepts of the rigorous KKR method, which is used to calculate the optical response of multiply interacting 3D periodic arrangements of NPs. In section "Results and Discussion", we show the results obtained for the parameters corresponding to those films fabricated in [2, 3]. Using the analytical method, we obtain a simple scale law for the plasmon resonance shift as a function of the average distance between particles and compare it with the results obtained by the KKR, focusing our attention on the cases described in [2, 3]. Theoretical and experimental results are compared in section "Optical Filters", where we also show that these films can be used for optical tuning by varying the NPs radius and the average distance between them. Finally, concluding remarks are given in section "Conclusions".

Theoretical Methods

In this section, we present the two theoretical models employed in this paper. In both models, we consider that all the Au NPs have the same radius a and are distributed in a periodic arrangement of period d (center-to-center distance between adjacent NPs) and embedded in a homogeneous medium. Taking into account that for the system under study, the geometrical parameters satisfy the relationship $a < d << \lambda$, where λ is the incident wavelength; the first approach proposed is based on a simple quasi-static model of interacting dipoles, which allows us to obtain an analytical expression for the evolution of the plasmon resonance wavelength as a function of the separation distance d. In this simple approach, we consider two systems: a one-dimensional chain of spheres (1D) and a single planar layer of periodically arranged spheres (2D). The second method is the KKR, which is a rigorous numerical tool that takes into account the full 3D arrangement of nanoparticles and their multiple interactions.

Quasi-static Model

This theoretical model is based on the quasi-static approximation, by which it is possible to find an analytical expression for the dependency of the plasma frequency as a function of the geometrical parameters of a 1D or 2D arrangement of metallic NPs [28, 29].

Since the relationship $\lambda >> d > a$ holds, the complex electromagnetic system of multiple NPs can be considered

as a system of interacting dipoles. In the framework of the quasi-static approximation, the near electric field generated by an oscillating point dipole $\mathbf{p}$ evaluated at an observation point $\mathbf{r}$ ($\mathbf{E}_{dip}$) is given by

$$\mathbf{E}_{dip} = \frac{1}{4\pi\epsilon_0}\left\{\frac{3\hat{n}(\mathbf{p}.\hat{n}) - \mathbf{p}}{r^3}\right\}, \quad (1)$$

where $\hat{n}$ is the unit vector in the direction of the observation point and then $\mathbf{r} = r\hat{n}$. In Eq. 1, retardation effects have been omitted. To estimate the dependency of the spectral position of the plasmon resonance on the geometrical parameters of the array, we followed the works by Kravets et al. [28] and Pinchuk et al. [29], who proposed a simple model to find this dependency for a Au 1D arrangement of metallic NPs.

To find the collective excitation or plasma frequency in an electromagnetically coupled system, we consider perturbations in the free electron *eigenmode* caused by electromagnetic fields induced by the nearest NP neighbors. The equation of motion for any free electron confined in the volume of the NP is $m\frac{d^2\mathbf{r}}{dt^2} = -e\left(\mathbf{E}_i^{Pol} + \sum_{j\neq i}\mathbf{E}_j^{Sca}\right)$ where m is the electron mass, $\mathbf{E}_i^{Pol} = -\mathbf{p}_i/3\epsilon_0 V$ (V is the volume of the metallic NP), $\mathbf{E}_j^{Sca}$ (the scattered electric field from the jth particle) has the functional form given by Eq. 1, e is the electron charge, and the sub-index j runs over all the dipoles of the system. In first approximation, only the contributions of the nearest neighbors are considered, that is, $j = i \pm 1$. For a linear array of NPs (see scheme in Fig. 1a (i)), we consider a plane electromagnetic wave at normal incidence with the electric field parallel to the x-axis (this condition will be used in the rest of the examples); the electric field scattered by the jth particle, evaluated at the position of the ith NP, is $\mathbf{E}_j^{Sca} = \frac{2\mathbf{p}_j}{4\pi\epsilon_0 d^3}$, where $\mathbf{p}_{j=i\pm1} = -neV\hat{x}$, and n is the concentration of free electrons in the system, and e is the electron charge. The resulting *eigenmode* lies along the x-axis [28] and the plasma frequency ω_{sp} is given by $\omega_{sp} = \omega_0\sqrt{1 - \frac{1}{2}\left(\frac{D^3}{d^3}\right)}$, where ω_0 is the surface plasmon resonance frequency of the isolated particle ($\omega_0 = \omega_p/\sqrt{3}$, and ω_p is the volume plasmon resonance frequency) and $D = 2a$ is the diameter of the NPs. The eigenmode wavelength, λ_{sp}, is related to its frequency by the following formula: $\omega_{sp} = 2\pi c/\lambda_{sp}$, where c is the speed of light in a vacuum. Then, from the equation for ω_{sp}, we obtain

$$\Lambda_{sp} = \frac{\lambda_{sp}}{\lambda_0} = \frac{1}{\sqrt{1 - \frac{1}{2}\left(\frac{D^3}{d^3}\right)}}. \quad . \quad (2)$$

Here, λ_0 represents the surface plasmon resonance wavelength associated with an isolated NP immersed in the same medium in which the NP array is embedded. Λ_{sp} provides an expression of the relative variation of the resonant wavelength of the system with respect to the spectral position of the resonant wavelength of an isolated NP [28, 29].

Applying the same procedure, we obtain the expression of the relative variation of the resonant wavelength for a hexagonal 2D configuration. For this geometry, six first neighbors are considered around the ith particle. Two of them are located along the x-axis; the other four have unit vectors $\hat{n} = \left[\pm 1/2, \pm\sqrt{3}/2\right]$.

When each of these unit vectors is replaced in Eq. 1, the scattered electric near field due to the jth neighbor at the position of the ith NP is obtained. The total electric incident field on the ith NP is calculated summing up the scattered fields of the six neighbors. For a polarization in the x direction, we have for Λ_{sp}^{hex} (see Fig. 1a (ii))

$$\Lambda_{sp}^{hex} = \frac{\lambda_{sp}}{\lambda_0} = \frac{1}{\sqrt{1 - \frac{1}{8}\left(\frac{D^3}{d^3}\right)}}, \quad (3)$$

whereas for a 2D square arrangement of NPs (Fig. 1a (iii)), we consider four first neighbors along the x and y axes, and four second neighbors with $\hat{n} = \sqrt{2}/2\,[\pm1, \pm1]$. Replacing these unit vectors in Eq. 1 as in the hexagonal case, we obtain

$$\Lambda_{sp}^{sq} = \frac{\lambda_{sp}}{\lambda_0} = \frac{1}{\sqrt{1 - \frac{1}{4}(\frac{D^3}{d^3}) - \frac{1}{4}\left[\frac{D^3}{(\sqrt{2}d)^3}\right]}} \quad . \quad (4)$$

It is interesting to note that the three expressions of Λ_{sp} given in Eqs. 2–4 have the same functional dependency, of the form

$$\Lambda_{sp}^{fit} = \left[1 - A\left(\frac{D^3}{d^3}\right)\right]^{-0.5} \quad , \quad (5)$$

which only depends on the geometrical ratio D/d (A is a constant). In particular, for this approximation, the resonance frequencies for hexagonal and square arrays do not change if the dipole moment vector (or incident electric field) is oriented along the x- or the y-axis. This constitutes the main contribution of this model, since it establishes the functional form of the non-linear behavior of the plasmon resonance wavelength with the distance between particles.

KKR Method

The second method employed for the simulation of the optical properties of NP films is the KKR, which is a rigorous method that has proved to be successful to compute the electromagnetic response of 3D arrangements of spheres immersed in a given dielectric medium. Within the KKR method, the electromagnetic interactions between

the scatterers are calculated by means of the layer-multiple-scattering method for spherical particles [22, 23]. The 3D NP film can be considered as a stack of parallel layers formed by spheres periodically arranged in a 2D lattice. To solve the electromagnetic problem, the multiple scattering between spheres of each single layer is calculated first. Then, the scattered response of multiple layers is determined by using a procedure similar to the one used to calculate the reflection and transmission properties of stratified media with planar interfaces. The transmittance (reflectance) is defined as the total transmitted (reflected) power normalized to the incident power. The absorption is obtained from the calculated transmittance and reflectance, by imposing the conservation of energy. The definitions of these quantities and the complete derivation can be found in [22].

It is important to remark that within the KKR method there are no limitations about the incidence angle and polarization of the incident light. This method has been extensively used to calculate the optical properties of photonic crystals [22, 23] and the electromagnetic response of colloidal crystals, as well as of metal-dielectric systems, and it was shown to be numerically efficient and robust even at high frequencies [24, 27]. In this paper, we use the KKR method to predict the plasmon resonance shift as the distance between NPs is varied, and also to calculate the transmittance spectra.

Results and Discussion

Plasmon Resonant Wavelength Shifts

In this section, we theoretically reproduce the behavior observed by Dalfovo et al. [2, 3] which described the use of Tetraoctylammonium bromide (TOABr)-coated Au NPs as colorimetric sensors and the role of coupling effects during exposure of the films to volatile organic compounds (VOCs). In these reports, it was determined that according to the polarity of the vapor, the LSPR sensor responds either shifting the plasmon wavelength to blue or red. For instance, in the presence of Tol, the plasmon wavelength blueshifts with respect to that of the unexposed films and this shift is associated with small separations between Au NPs caused by significant coupling effects. They assumed that separation/shrinkage between Au NPs was caused by the partition of analyte vapors into the organic matrix leading to film swelling/contraction [2]. To prove this experimentally, GISAXS was performed and it was observed that the inter-NP distance within the film increases $\approx$ 0.5 nm in the presence of Tol vapors [2].

In order to model the electromagnetic interaction between Au NPs within the film and predict their electromagnetic response, here we employ the theoretical approaches described in section "Theoretical Methods". For the QS, we consider three different geometrical configurations of NPs which correspond to a one-dimensional (1D) crystal (i), a 2D periodic arrangement of NPs distributed in a hexagonal lattice (ii), and in a square lattice (iii), as shown in Fig. 1a. We compare these results with a more realistic calculation for a slab comprising an array of spheres with a ratio $d/D = 1.8$, which is the value measured in the experimental films.

Figure 1b plots the evolution of the relative plasmon resonant wavelength $\Lambda_{sp} = \lambda_{sp}/\lambda_0$ as a function of d/D calculated with the quasi-static approximation for the three geometrical configurations shown in Fig. 1a. The results of the QS for configuration (iii) are compared with those obtained by means of the KKR for a slab of thickness d comprising a single layer of Au spheres embedded in a dielectric medium with permittivity $\epsilon_m = 2.25$. This value has been chosen taking into account the estimation made in [2] for Au NP films. The dielectric permittivity of gold was obtained from the Johnson and Christy experimental data [30]. We also include the results obtained for the same slab using the MG approximation. To calculate the value of λ_0 for the KKR and the MG results, we simulated an isolated NP immersed in a slab of ϵ_m, by considering the same slab but with a lattice constant $d = 20$ nm, which yields $\lambda_0 = 533$ nm.

For all the geometrical configurations considered, it is clear from Fig. 1b that as the NPs come closer together ($d \rightarrow D$), the relative resonant wavelength exhibits significant increments. It is interesting to note that the results obtained by the approximate quasi-static model for a 1D and for a 2D array (square or hexagonal) follow a trend similar to those of the KKR method and of the MG approximation. However, the evolution of the plasmon wavelength obtained by the KKR method deviates from that predicted by the QS method. This is to expect since the QS does not take into account multiple interactions between particles (long-range interaction), which might be significant for particles that are close to each other.

In Fig. 1c, we show the evolution of the resonant plasmon wavelength for both KKR and MG methods. As expected, the KKR results agree very well with those obtained by the MG for low values of the filling fraction, which in our system correspond to large values of d/D. For small values of d/D, the filling fraction increases, and then higher order interactions play a role in the electromagnetic response of the system. In Fig. 1c, we observe a good agreement between both methods for $d/D > 1.6$, approximately.

It is well known that the MG method is based on the quasi-static approximation. Therefore, the MG results

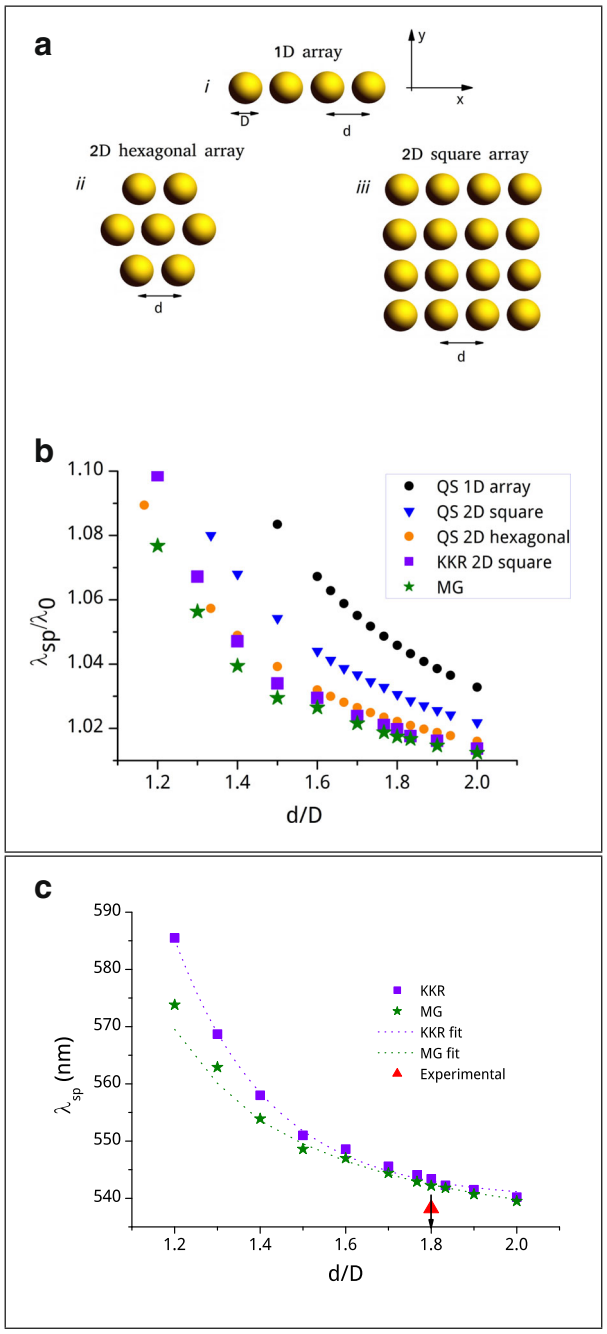

Fig. 1 Schemes of the arrangements of spherical Au NPs of diameter (D) studied: one dimensional (1D) (i), 2D hexagonal (ii), and 2D square crystal (iii) array (a). In all three cases, the structures are perfectly periodic with lattice constant d. Evolution of the relative dipolar plasmon wavelength as a function of the geometrical ratio d/D computed with QS, KKR, and MG: QS for a 1D array (black solid circles), QS for a 2D square lattice (blue inverted triangles), QS for a 2D hexagonal lattice (orange circles), KKR for a slab comprising a 2D square lattice of NPs immersed in a dielectric medium (violet squares), and MG for the same slab (green stars) (b). Plasmon resonant wavelength as a function of d/D calculated with the KKR and the MG (c). In dotted line, we show the fitting function for the KKR (violet) and for the MG (green) results. The black arrow indicates the estimated experimental value $d/D = 1.8$, and the red triangle indicates the experimental plasmon resonant wavelength obtained in [2]

shown in Fig. 1c can be fitted by a function of the form (5) with $\lambda_0 = 533$ nm and A = 0.2 (green dotted line). On the other hand, the KKR results cannot be fitted by a function of this form. Instead, the best fit (shown in violet dotted line) is obtained by a decreasing exponential function of the form:

$$\Lambda_{sp}^{fit} = y_0 + Be^{[-(d/D)/t]} \ , \tag{6}$$

with $y_0 = 539$ nm, $B = 9585$ nm, and $t = 0.22$, with values of t being consistent with those found in Ref. [10] for dimers. Equation 6 can be used to study the plasmon wavelength shift as a function of d/D.

In the figure, we also include the experimental $\lambda_{sp} = 538.21$ nm (red triangle) for the fabricated films reported in Refs. [2, 3]. Taking into account that in these films the Au NPs have a diameter of $D \approx 3.0$ nm and the core-to-core distance of $d \approx 5.4$ nm, the experimental d/D is approximately 1.8.

In Fig. 2, we use the KKR method to evaluate the plasmon shift behavior observed in [2, 3]. To model this system, we considered the same slab as in Fig. 1b and c. As the film is exposed to Tol or EtOH vapors, the arrays of NPs react. In Fig. 2, we represent this situation: with horizontal solid and dotted line, we denote the plasmon resonance wavelength at the initial and final states, respectively. Figure 2a represents the changes in a film initially exposed to N_2 gas and then to Tol vapors, which caused an increase in d/D from 1.8 to 1.9. Since we consider that the NP diameter remains constant, the increase in d/D is solely due to an increase in the distance between NPs within the film (see inset in Fig. 2a). For this case, the relative plasmon resonance wavelength obtained by the KKR method is $\lambda_{sp}^f/\lambda_{sp}^i = 0.996$ (f and i denote final and initial states, respectively), i.e., we get a blueshift of the plasmon resonance wavelength. This theoretical value is in good agreement with the experimental shift that was 0.997 (see Ref. [3]).

Figure 2b illustrates the results for the same Au NPs within the same structure considered in Fig. 2a but now exposed to EtOH vapors. In this case, the geometrical parameter d/D decreases from 1.833 to 1.767 in the presence of EtOH (shown in vertical lines), indicating that the NPs approach each other, as schematized in the inset of Fig. 2b. Therefore, according to the KKR method, $\lambda_{sp}^f/\lambda_{sp}^i = 1.004$, indicating a redshift of the plasmon peak, although this value is slightly smaller than the experimental displacement that is 1.006 (see Ref. [3]).

As shown in [2], when the film is exposed to Tol, the NPs move away from each other, causing a blueshift of the resonant wavelength, whereas in the presence of EtOH, the NPs approach each other and this leads to a redshift of the plasmon resonance. The different vapors produce opposite behaviors in the movement of the NPs, which,

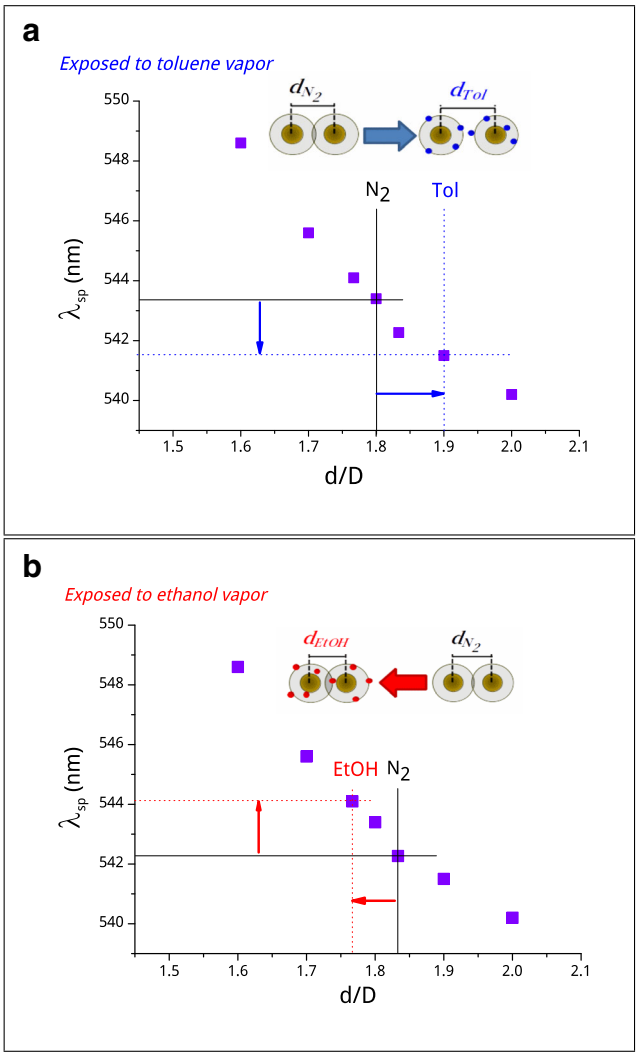

Fig. 2 Calculated plasmon wavelengths obtained with the KKR method as a function of the geometrical parameter d/D, for a slab comprising a single layer of NPs exposed to Tol (**a**) and EtOH (**b**) vapors. Horizontal solid and dotted lines denote the plasmon resonant wavelength at the initial and final stages, respectively. The insets in each panel represent a minimalistic system composed of only two Au NPs that separate or get closer together depending on the type of analyte vapors

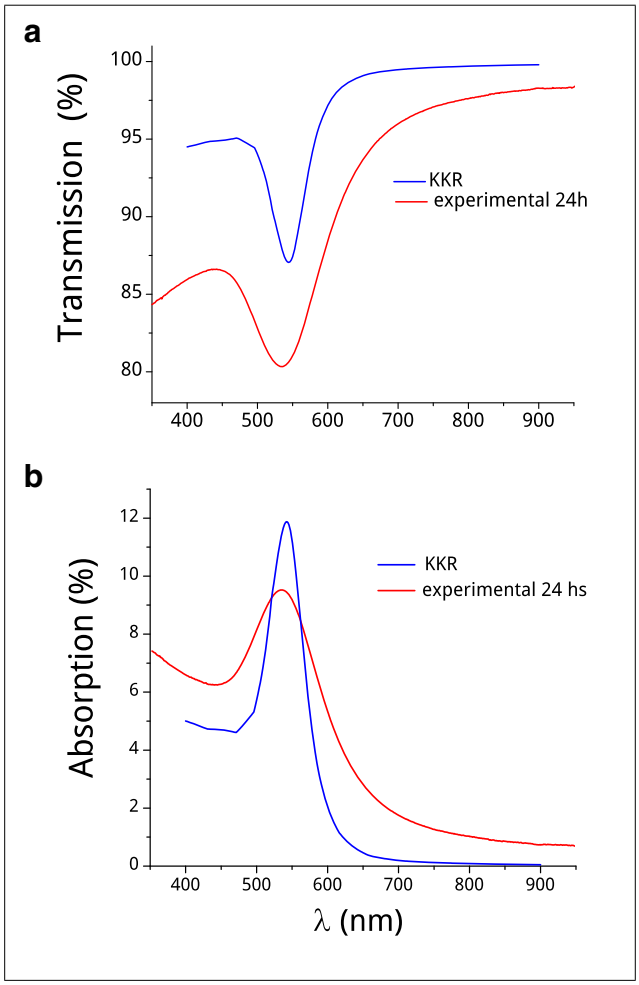

Fig. 3 Calculated and experimental transmission and absorption spectra for $d/D = 1.8$

in turn, produce opposite shifts in the plasmon resonance wavelength. Therefore, for films exposed to the non-polar and polar vapors shown in Fig. 2, the theoretical values obtained for the relative resonance plasmon wavelengths exposed to Tol and EtOH follow the same trend than the experimental values observed in Ref. [2].

Optical Filters

In Fig. 3a and b, we present experimental and KKR absorption and transmission spectra. For the KKR simulations, we used the same slab modelled in the previous figure for $d/D = 1.8$. The experimental curves correspond to a film incubated for 24 h. It can be observed that our theoretical model reproduces quite well the main features of the optical response of the fabricated film. The theoretical curves show the same behavior that the experimental ones, although the transmission minimum in Fig. 3a and the absorption peak in Fig. 3b calculated theoretically are slightly redshifted with respect to the corresponding measured curves. Besides, the theoretical half-widths are smaller than the experimental ones.

The differences between the theoretical and the experimental results can be attributed to deviations of the model from the actual film, such as the geometry of the arrangement, the size and shape of the NPs, the eventual formation of clusters of NPs, and the constitutive parameters of the materials involved. In particular, the dielectric function used to model the Au NPs does not take into account size corrections. It is known that the absorption spectrum for an isolated Au nanoparticle widens significantly if the appropriate corrections are introduced [31–33].

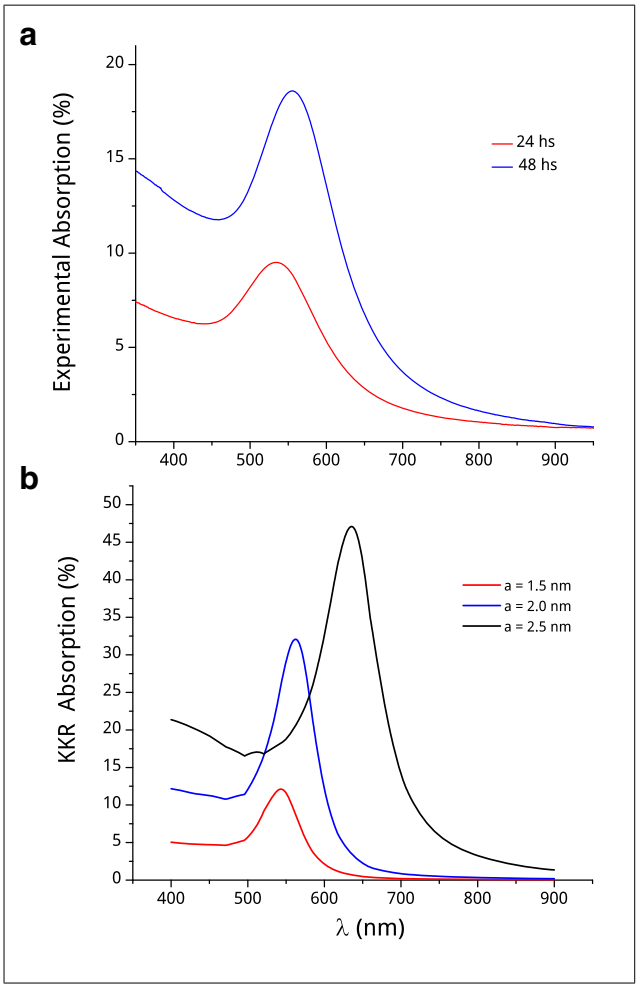

Fig. 4 **(a)** Experimental absorption spectra for different incubation times of the film: 24 h (red line) and 48 h (blue line). **(b)** Theoretical absorption spectra (KKR method) for $d = 5.4$ nm and for two different values of the Au NP radius: $a = 1.5$ nm (red line), $a = 2.0$ nm (blue line), and $a = 2.5$ nm (black line)

In Fig. 4a, we show the experimental absorption spectrum for two different incubation times of the film, 24 h (red line) and 48 h (blue line). Both experimental curves show a similar behavior; the peak for the 48-h film is higher and slightly redshifted with respect to that of the 24-h film. Notice that the thickness of the films increases with the incubation time and also that the Au NPs tend to form clusters, which eventually can be regarded as an increase of the effective size of the NPs. To investigate the possible influence of the NP size on the optical response, in Fig. 4b, we show the absorption spectra obtained by the KKR method for a film with $d = 5.4$ nm, for different values of the NP radius a. Our theoretical results show that as a is increased (keeping d fixed), the absorption peak redshifts and its intensity is enhanced. The behavior of the theoretical curves as the NPs become larger is similar to that observed for the experimental films as the incubation time increases. Therefore, the Au NP slab employed to model the actual films seems to represent quite well the main features of the experimental absorption spectra.

Conclusions

In summary, we have confirmed via calculations that the plasmon resonance wavelength of NP films exposed to EtOH and Tol vapors shift to red or blue consistently with a shrinkage or separation of the Au NPs, respectively, which also confirms that coupling effects are predominant. We have applied the QS and the KKR method to investigate the dependency of the resonant wavelength with the geometrical parameter d/D. Even though the quasi-static model predicted the correct behavior, the KKR method could better reproduce the experimental results. The KKR approach proved to be an effective tool for estimating the spectral position of the absorption peaks of the fabricated films and then it could be employed as a design tool.

Finally, taking into account that small changes in the inter-NPs distance cause significant modifications in the optical transmission, we have shown that these films can perform as optical filters. Research on optimization of such films for applied devices such as VOC detectors and optical filters is being carried out and will be published soon.

Acknowledgments The authors of this article would like to sincerely thank to Lic. Christian D'Ambrosio, who implemented the MG model and performed part of the calculations with the KKR method for this paper.

Funding Information F.I.J. and D.M.C. acknowledge the financial support from International Cooperation Project (CONICET-NSF) for student and professor exchange between the University of Louisville (KY, USA) and Universidad de La Plata. F.I.J. acknowledge the financial support from Agencia Nacional de Promoci'on cient'ifica y tecnol'ogica PICT 2016-1377. M.L. acknowledges partial support from Universidad Nacional del Centro de la Provincia de Buenos Aires and from the Comisión de Investigaciones Científicas de la CIC-PBA - Programa de fortalecimiento de centros de Investigación 2017. D.S and M.I. acknowledge partial support from Universidad de Buenos Aires (UBACyT 20020150100028BA).

References

1. Ghosh SK, Pal T (2007) Interparticle coupling effect on the surface plasmon resonance of gold nanoparticles: from theory to applications. Chem Rev 107:4797–4862
2. Dalfovo MC, Salvarezza RC, Ibañez FJ (2012) Improved vapours selectivity and stability of localized surface plasmon resonance with a surfactant-coated Au nanoparticles film. Anal Chem 84:4886–4892
3. Dalfovo MC, Giovanetti LJ, Ramallo-López JM, Salvarezza RC, Requejo FG, Ibañez FJ (2015) Real-time monitoring distance changes in surfactant-coated Au nanoparticle films upon volatile organic compounds (VOCs). J Phys Chem C 119:5098–5106

4. Kessentini S, Barchiesi D, D'Andrea C, Toma A, Guillot N, Di Fabrizio E, Fazio B, Maragó OM, Gucciardi PG (2014) Gold dimer nanoantenna with slanted gap for tunable LSPR and improved SERS. J Phys Chem C 118:3209–3219
5. Song Y, Tran VT, Lee J (2017) Tuning plasmon resonance in magnetoplasmonic nanochains by controlling polarization and interparticle distance for simple preparation of optical filters. ACS Appl Mater Interfaces 9:24433–24439
6. Meriaudeau F, Downey T, Wig A, Passian A, Buncick M, Ferrell TL (1999) Fiber optic sensor based on gold island plasmon resonance. Sens Actuators B 54:106–117
7. Singh MP, Strouse GF (2010) Involvement of the LSPR spectral overlap for energy transfer between a dye and Au nanoparticle. J Am Chem Soc 132:9383–9391
8. Rechberger W, Hohenau A, Leitner A, Krenn JR, Lamprecht B, Aussenegg FR (2003) Optical properties of two interacting gold nanoparticles. Opt Commun 220:137–141
9. Haynes CL, McFarland AD, Zhao LL, Van Duyne RP, Schatz GC, Gunnarsson L, Prikulis J, Kasemo B, Kall M (2003) Nanoparticle optics: the importance of radiative dipole coupling in two-dimensional nanoparticle arrays. J Phys Chem B 107:7337–7342
10. Jain PK, Huang W, El-Sayed MA (2007) On the universal scaling behavior of the distance decay of plasmon coupling in metal nanoparticle pairs: a plasmon ruler equation. Nano Lett 7:2080–2088
11. Jenkins JA, Zhou Y, Thota S, Tian X, Zhao X, Zou S, Zhao J (2014) Blue-shifted narrow localized surface plasmon resonance from dipole coupling in gold nanoparticle random arrays. J Phys Chem C 118:26276–26283
12. Agrawal VV, Varghese N, Kulkarni GU, Rao CNR (2008) Effects of changes in the interparticle separation induced by alkanethiols on the surface plasmon band and other properties of nanocrystalline gold films. Langmuir 24:2494–2500
13. Sendroiu IE, Mertens SFL, Schiffrin DJ (2006) Plasmon interactions between gold nanoparticles in aqueous solution with controlled spatial separation. Phys Chem Chem Phys 8: 1430–1436
14. Reinhard BM, Siu M, Agarwal H, Alivisatos AP, Liphardt J (2005) Calibration of dynamic molecular rulers based on plasmon coupling between gold nanoparticles. Nano Lett 5:2246–2252
15. Hill RT, Mock JJ, Hucknall A, Wolter SD, Jokerst NM, Smith DR, Chilkoti A (2012) Plasmon ruler with angstrom length resolution. ACS Nano 6:9237–9246
16. Ross MB, Mirkin CA, Schatz GC (2016) Optical properties of one-, two-, and three-dimensional arrays of plasmonic nanostructures. J Phys Chem C 120:816–830
17. Kelly KL, Coronado E, Zhao LL, Schatz GC (2003) The optical properties of metal nanoparticles: the influence of size, shape, and dielectric environment. J Phys Chem B 107:668–677
18. Zhao J, Pinchuk AO, McMahon JM, Li S, Ausman LK, Atkinson AL, Schatz GC (2008) Methods for describing the electromagnetic properties of silver and gold nanoparticles. Acc Chem Res 41:1710–1720
19. Nordlander P, Oubre C, Prodan E, Li K, Stockman MI (2004) Plasmon hybridization in nanoparticle dimers. Nano Lett 4:899–903
20. Halas NJ, Lal S, Chang W-S, Link S, Nordlander P (2011) Plasmons in strongly coupled metallic nanostructures. Chem Rev 111:3913–3961
21. Modinos A (1987) Scattering of electromagnetic waves by a plane of spheres-formalism. Phys Stat Mech Its Appl 141:575–588
22. Stefanou N, Yannopapas V, Modinos A (1998) Heterostructures of photonic crystals: frequency bands and transmission coefficients. Comput Phys Commun 113:49–77
23. Yannopapas V, Modinos A, Stefanou N (1999) Optical properties of metallodielectric photonic crystals. Phys Rev B 60:5359–5365
24. Dorado LA, Depine RA, Míguez H (2007) Effect of extinction on the high-energy optical response of photonic crystals. Phys Rev B 75(241101)
25. Ruppin R (2000) Evaluation of extended Maxwell-Garnett theories. Op Comm 108:273
26. Koledintseva M, DuBroff R, Schwartz R (2006) A Maxwell Garnett model for dielectric mixtures containing conductin particles at optical frequencies. Progress in Electromagnetics Research PIER 63:223
27. Ortiz G, Inchaussandague M, Skigin D, Depine R, Mochán WL (2014) Effective non-retarded method as a tool for the design of tunable nanoparticle composite absorbers. J Opt 16:105012
28. Kravets VV, Yeshchenko OA, Gozhenko VV, Ocola LE, Smith DA, Vedral JV, Pinchuk AO (2012) Electrodynamic coupling in regular arrays of gold nanocylinders. J Phys Appl Phys 45(045102)
29. Pinchuk AO, Schatz GC (2008) Nanoparticle optical properties: far- and near-field electrodynamic coupling in a chain of silver spherical nanoparticles mater. Sci Eng B 149:251–258
30. Johnson PB, Christy RW (1972) Optical constants of the noble metals. Phys Rev B 6:4370
31. Scaffardi LB, Tocho JO (2006) Size dependence of refractive index of gold nanoparticles. Nanotechnology 17:1309–1315
32. Scaffardi LB, Schinca DC, Lester M, Videla FA, Santillán JM, Abraham Ekeroth RM (2013) Size-dependent optical properties of metallic nanostructures, uv-vis and photoluminescence spectroscopy for nanomaterials characterization. In: Challa Kumar (ed)
33. Abraham bad RM, Lester M (2013) Optical properties of silver-coated silicon nanowires. Morphol Plasmonic Excit Plasmon 8:1417–1428